ROYAL SOCIETY
OF CHEMISTRY

PAPER

Check for updates

Ultralong room temperature phosphorescence and ultraviolet fluorescence from simple triarylphosphine oxides†

Satyam Jena, Akkarakkaran Thayyil Muhammed Munthasir and
Pakkirisamy Thilagar (ID) *

Achieving persistent room-temperature phosphorescence in halogen/heavy atom-free organic compounds is challenging due to the ultrafast deactivation of excited states. This study reports the ultralong room temperature phosphorescence (ULRTP) from simple triarylphosphine oxides. Although phosphine/oxides have been known for several decades and have been well exploited in catalysis, surprisingly, the ULRTP properties of these simple compounds have never been explored. The luminescence characteristics of triarylphosphines (**1–4**) and triarylphosphine oxides (**5–8**) were fine-tuned by systematically varying the steric crowding around the phosphorus center. Phosphines **1–4** show room temperature phosphorescence (RTP) with a 4.30–5.45 microsecond lifetime, while phosphine oxides **5–8** exhibit persistent RTP with millisecond lifetimes. ULRTP was observed only for the crystalline solids of **5–8** and was not observed for amorphous ground samples and thin films. Detailed steady-state, time-resolved photoluminescence (PL), crystal structure and computational studies collectively implied that the intermolecular interactions are essential for ULRTP in **5–8**.

Introduction

Ultralong/persistent room-temperature phosphorescence (ULRTP/pRTP) is the radiative depopulation of the lowest triplet excited state (T_1) to the singlet ground state (S_0) with a lifetime of more than 100 ms.[1] In recent years, ULRTP/pRTP materials have been increasingly utilized in OLEDs, security writing, sensing, phosphorescence live-cell imaging, *etc.*[2–19] According to quantum mechanics, nonradiative $S_1 \rightarrow T_n$ intersystem crossing (ISC) and radiative $T_1 \rightarrow S_0$ phosphorescence processes are spin-forbidden.[20,21] Thus, the phosphorescence phenomenon has been considered exclusive for inorganic complexes with strong spin–orbit coupling (SOC).[22–28] As SOC is weaker in organic molecules with lighter elements, they rarely exhibit phosphorescence at room temperature. Recently, theoretical calculations using the hybrid quantum mechanics and molecular mechanics (QM/MM) model revealed that organic compounds containing n/π-groups facilitate the long-lived afterglow efficiency.[29]

Lately, strategies such as (i) inclusion of halogen atoms (Cl, Br, I, *etc.*) and (ii) introduction of the carbonyl moiety or heteroatoms having a lone pair of electrons (O, S, N, P, Se, *etc.*) have been put forth to increase the rate of ISC in organic luminophores.[30–42] Strong SOC may enhance the rate of the ISC process; however, in that case, radiative decay will be very fast, resulting in a shorter phosphorescence lifetime.[43,44] Hence, achieving persistent organic RTP continues to be a challenging task.

Nevertheless, innovative molecular designs have been developed to attain organic ultralong RTP (ULRTP) in recent years; to mention a few, Huang and coworkers exploited intramolecular triplet–triplet energy transfer to boost the efficiency of ULRTP.[45] Bryce *et al.* demonstrated a red emissive carbazole containing carbonyl compound exhibiting ultralong phosphorescence with a lifetime of 280 ms.[46] Adachi *et al.* developed ULRTP by exploiting host–guest chemistry to minimize radiation-less energy loss.[47] Fukushima *et al.* reported a library of simple aryl boronic esters exhibiting long-lived room temperature phosphorescence with a lifetime of up to 1.85 s.[48] Very recently, Marder *et al.* uncovered the ultralong luminescence in simple triaryl boranes by controlling $(\sigma, B_p) \rightarrow (\pi, B_p)$ transitions.[49] Despite these efforts, ULRTP materials are scarce in the literature.

On the other hand, organophosphorus compounds attracted special attention due to their unique molecular topology and easy chemical modification scope.[50–60] Among various

Department of Inorganic and Physical Chemistry, Indian Institute of Science Bangalore, 560012, India. E-mail: thilagar@iisc.ac.in
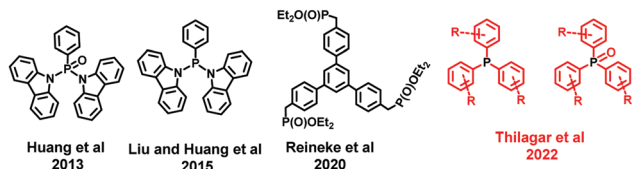
**Chart 1** Examples of phosphorus-based ultralong RTP molecules.

organophosphorus compounds, triarylphosphines and phosphine oxides have received much attention due to their potential applications in catalysis, materials, medicines, *etc.*[61–65] The tricoordinate phosphorus atom of phosphines has pyramidal geometry with a lone pair of electrons of strong s character.[66] The geometric and electronic features of the tricoordinate phosphorus atom favor n → π* transition and promote the spin forbidden S_1 → T_n intersystem crossing to populate triplet excited states.[67] For example, in 2015, Liu and Huang *et al.* manipulated lone pair electrons on phosphorus in arylphosphanediamines to promote the production of long-lived triplet excitons through n → π* transitions.[45] Furthermore, Huang and coworkers engineered the resonance bonding interaction between the P=X (X = O, S) moiety and nitrogen of the aromatic heterocyclic amines in phosphoramides for developing metal-free ultralong phosphors (Chart 1).[68,69]

Recently, Reineke *et al.* reported novel aryl phosphonates exhibiting blue ultralong room-temperature phosphorescence (Chart 1).[70] In 2021, Tang *et al.* reported the luminescence features of triphenylphosphine in solution and the crystalline state.[71] However, surprisingly, the delayed luminescence characteristics of simple triarylphosphine oxides have not been explored to date.

We have been involved in developing RTP materials for the last one decade.[33–35,72–79] As part of the ongoing program, we set to investigate the RTP characteristics of a series of simple triarylphosphines (**1**, **2**, **3**, and **4**) and triarylphosphine oxides (**5**, **6**, **7**, and **8**) to gain an understanding on how different are the lone pair electrons in R_3P compared to arylphosphanediamines in the production of triplet excitons through n → π* transitions, and to understand the difference between R_3P and $R_3P(O)$ based n → π* transitions in the production of triplet excitons. For this study, we synthesized a series of arylphosphines and arylphosphine oxides (Scheme 1). The molecular rigidity of these compounds was systematically tuned by changing the sterically demanding aryl moiety attached to the phosphorus atom. Interestingly, triarylphosphine oxides (**5**, **6**, **7**, and **8**) showed intriguing ULRTP in the solid state, and these results are presented in this article.

Results and discussion

Analytically pure **1** and **2** were obtained by repeated recrystallization of crystalline powders from commercial sources. Compounds **3** and **4** were synthesized by following modified literature procedures.[80] Oxidation of the phosphorus centers in **1**, **2**, **3**, and **4** with 30% H_2O_2 at 0 °C gave **5**, **6**, **7**, and **8** in
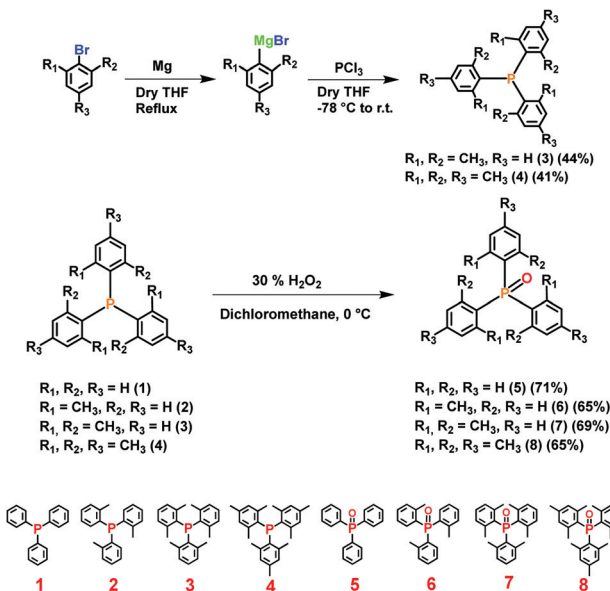
Scheme 1 Synthesis and molecular structures of compounds **1–8**. All compounds are designed keeping in mind that the lone pairs of electrons on heteroatoms (P and O) facilitate the rate of intersystem crossing (ISC) which leads to phosphorescence from triplet excited states.

quantitative yields, respectively (Scheme 1). Compounds **1–8** were characterized by NMR (^{1}H, ^{13}C, and ^{31}P), high-resolution mass spectrometry (HRMS), and elemental analysis (EA) (Fig. S1–S34, ESI†). The molecular structures of all these compounds were confirmed by single-crystal X-ray diffraction (SCXRD) analysis (Tables S1–S4, ESI†).

Optical studies

Hexane solutions of triaryl phosphines **1–4** showed broad absorption in the region of 250 nm to 370 nm. The absorption maximum progressively redshifted with increasing the steric crowding around the phosphorus center; a sizeable bathochromic shift was observed for xylyl (**3**) and mesityl (**4**) derivatives (Fig. 1a and b). In sharp contrast, triarylphosphine oxides **5**, **6**, **7**, and **8** exhibit structured absorption features in the region of 250 nm to 300 nm. The absorption of triarylphosphine oxides is blueshifted compared to the respective phosphines. The hypsochromic shift was maximum for xylyl (**7**) and mesityl (**8**) derivatives. Further, the molar absorptivity of oxides was significantly lower than that of the respective phosphines (Table S5, ESI†). Except for **1**, the absorption signatures of
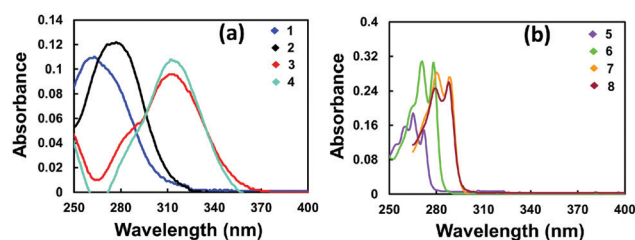

Fig. 1 (a) UV-visible absorption spectra of **1–4** in hexane (conc. 10^{-5} M). (b) UV-visible absorption spectra of **5–8** in hexane (conc. 10^{-4} M).

This journal is © The Royal Society of Chemistry 2022

J. Mater. Chem. C, 2022, **10**, 9124–9131 | **9125**

2–8 were insensitive to the solvent polarity indicating the nonpolar ground state in these compounds (Fig. S40–S43, ESI†).

DFT and TD-DFT computational studies were carried out on all the compounds to understand the nature of electronic transitions. The calculated singlet vertical transition energies ($S_0 \rightarrow S_1$ and $S_0 \rightarrow S_2$) along with their oscillator strengths and dominant transition configurations are listed in Table S9 (ESI†). Although the computed transition energies did not match the experimental values precisely, similar energy profile trends were observed in experimental and theoretical data (Fig. S91 and Table S9, ESI†).

The frontier molecular orbitals (FMOs) in **1–4** are delocalized over the entire molecules, except that the contribution of phosphorus (lone pair electron) is significantly larger in the HOMO and no phosphorus contribution in the LUMO (Fig. S92, ESI†). The HOMOs in **5**, **6**, and **8** are delocalized over aryl moieties with a significant contribution from the oxygen lone pair. In contrast, the HOMO in **7** is fully delocalized on xylyl moieties with no assistance from the P=O moiety. The LUMOs in **5**, **6**, **7**, and **8** are delocalized over the entire molecule; furthermore, the negative hyperconjugation has progressively prevailed in sterically demanding phosphine oxides (Fig. S93, ESI†).[81,82] These results implied that the repulsive interaction between the phosphorus lone pair electrons and the attached π-system elevated the HOMO energy in **1–4** compared to phosphine oxides **5–8**; consequently, phosphines absorb at a lower energy compared to the corresponding phosphine oxides. The computed oscillator strength for $S_0 \rightarrow S_1$ transitions in phosphine oxides is much lower than the value calculated for the corresponding phosphines. This result directly corroborates the weaker absorption features of phosphine oxides compared to phosphines (Tables S5 and S9, ESI†).

Phosphines **1** and **2** showed dual emission with a high energy sharp band peaking at ~290 nm and a broad structureless band at ~480 nm. In contrast, **3** and **4** showed a broad structureless fluorescence band at ~490 and 481 nm, respectively (Fig. 2a). Surprisingly, the phosphine oxides **5–8** are non-emissive in the solution state. Similar to the absorption spectra, the photoluminescence (PL) of **3** and **4** redshifted compared to **1** and **2**. Compounds **1–4** showed strong fluorescence with a bathochromic shift when the solvent polarity changed from hexane to methanol. This result indicated the polar nature of the emissive excited state in these compounds (Fig. S44 and S45, ESI†). The observed changes in the PL intensity of these compounds can be attributed to the difference in the solubility of these compounds in polar and nonpolar solvents.

Time-resolved decay kinetic studies on **1–4** showed a lifetime in the nanosecond range (Table S6a, ESI†). The PL λ_{max} in **1–4** is insensitive to solution concentrations, and the excitation spectra of these compounds obtained by monitoring the decay of respective emission maxima reproduced their absorption spectra (Fig. S46–S49, ESI†). These results indicated that **1–4** are fluorescent in the solution state and emit from the intramolecular S_1 excited state.

Pristine solids of **1–4** showed intense blue/cyan blue luminescence compared to solutions (Fig. 2c). Further, the solid-state PL spectra of these compounds are redshifted and have lower full-widths at half maximum than those of the solutions (Fig. 2b). The strong and sharp PL features can be attributed to the deactivation of nonradiative decay channels and line broadening through molecular motion in the solid state compared to the solutions. The emission maxima of phosphines remain the same when excited at different wavelengths in the region of 260 to 340 nm, indicating that they emit from the same electronic excited state, irrespective of excitation energy (Fig. S50, ESI†).

Upon excitation, with 340 nm light, phosphines **1–4** show delayed emission, matching the fluorescence spectra (Fig. S51 and S52, ESI†). The delayed luminescence bands redshifted for compounds **3** and **4** (~480 nm) compared to **1** and **2** (~440 nm). The triplet excited state lifetimes of these compounds are in the range of 4.30–5.45 μs at room temperature (Table S6a, ESI†). Compounds **1–4** showed intense phosphorescence at 77 K and the excited-state lifetime also increased to milliseconds, which is typical of RTP molecules (Fig. S59–S62 and Table S6a, ESI†).[35,40,49] The RTP characteristics of these compounds are in line with the RTP features of triphenylphosphine reported by Tang et al.[71]

Interestingly, unlike in solutions, compounds **5–8** showed intense PL (λ_{max}: 370–400 nm) with a weak shoulder peak at ~500 nm in the solid state. Furthermore, compounds **5–8** showed excitation wavelength-dependent emission features in sharp contrast to the PL of phosphines **1–4**. When excited in the wavelength range of 260 to 300 nm, compounds **5–8** showed a sharp PL band peaking at 290–320 nm with a shoulder at 330–360 nm (Fig. S53–S56, ESI†). However, no phosphorescence was observed for these compounds when excited at 260 nm. The PL quantum yields and radiative (K_r) and nonradiative decay constants (K_{nr}) are summarized in Table S7 (ESI†). These results indicated that the phosphines are brighter luminophores than the respective phosphine oxides. Time-resolved decay studies on these molecules revealed a nanosecond lifetime for fluorescence and a millisecond lifetime for phosphorescence (Table S6b, ESI†).

Variable temperature PL and time-resolved decay kinetics of these compounds have shown that, at a lower temperature,
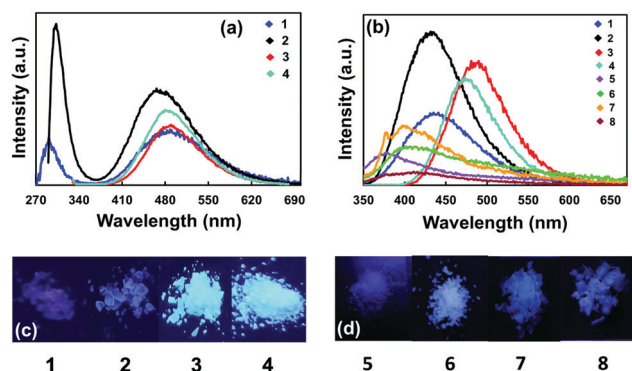

Fig. 2 Photoluminescence spectra of **1–4**: (a) chloroform solutions (conc. 10^{-5} M) and (b) crystals of **1–8** (λ_{ex} = 320 nm) at room temperature. (c and d) Digital photographs of pristine solids of **1–8** under 365 nm UV light illumination and ambient conditions.

9126 | J. Mater. Chem. C, 2022, **10**, 9124–9131

This journal is © The Royal Society of Chemistry 2022

both the PL intensity (fluorescence with resolved vibronic transitions and phosphorescence) and lifetimes were enhanced significantly than those at room temperature (Fig. S57, S66 and Table S6b, ESI†). Furthermore, the excitation spectra of PL bands reproduced their absorption spectra (Fig. S67 and S68, ESI†). The energy of fluorescence and phosphorescence peaks matched well with the individual molecules' computed S_1 and T_1 energies (Tables S12 and S13, ESI†). These results suggested that the fluorescence and phosphorescence of these compounds are from the S_1 and T_1 electronic states emerging from single molecular species and not intermolecular aggregates. The absence of fluorescence bands in dilute solutions and strong solid-state fluorescence indicate that the radiative decay process in these molecules is susceptible to molecular motions.

Intriguingly, when excited at wavelengths in the 320 to 400 nm range, these compounds showed a new set of fluorescence and phosphorescence bands in the regions of 370–430 and 480–550 nm, respectively (Fig. 3 and Fig. S53–S56, S73, and S74, ESI†). Time-resolved PL studies showed that the lifetimes of fluorescence (370–430 nm) and phosphorescence bands (480 nm to 550 nm) are longer than the lifetimes of the PL band in the region of 290–320 nm ((λ_{ex} = 260 to 300 nm)) (Table S6b and Fig. 4, ESI†). The RTP band was progressively red-shifted with increasing the number of methyl substituents on the phenyl moieties attached to the phosphorus center (482 nm for **5**, 523 nm for **6**, 543 nm for **7**, and 549 nm for **8**). Both the PL intensities and lifetimes of these compounds increased manifold at low temperatures, typical of room temperature phosphorescence compounds.[37]

The excitation spectra obtained by monitoring the decay of the PL maximum of lower energy bands were red-shifted and significantly different from their absorption spectra (Fig. S69–72, ESI†). The lower energy PL bands did not appear when excited in the region of 260 to 300 nm, corresponding to the
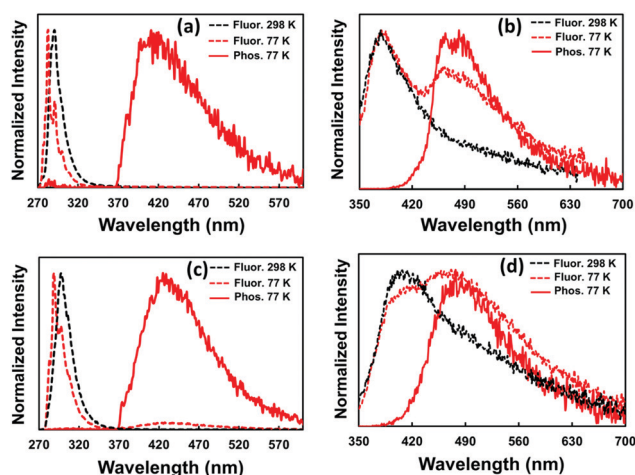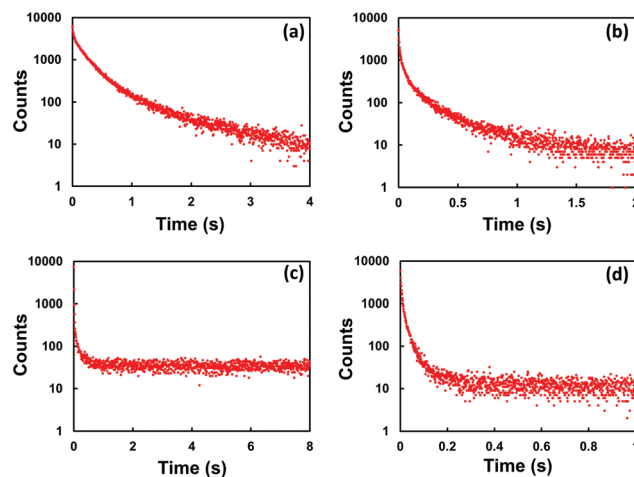

Fig. 4 Phosphorescence decay of the as-prepared crystals of **5** (λ_{em} = 500 nm) (a), **6** (λ_{em} = 520 nm) (b), **7** (λ_{em} = 530 nm) (c), and **8** (λ_{em} = 520 nm) (d) at λ_{ex} = 340 nm with a 100 µs delay at room temperature under a N_2 atmosphere.

electronic absorption of phosphine oxide monomers. The PL bands at 370–430 nm and 480–550 nm appeared selectively when crystalline samples of **5–8** were excited in the 320 to 360 nm region corresponding to intermolecular aggregates. Furthermore, the amorphous powders of **5–8** do not show lower energy bands at 480–500 nm. These results collectively point to the fact that the lower energy PL occurs from the S_1 and T_1 electronic states emerging from intermolecular aggregates rather than monomeric molecular species.[84–86] The phosphorescence band in **5** was quenched when recorded under an O_2 atmosphere; however, **6**, **7**, and **8** showed minor changes in the phosphorescence intensity under similar conditions (Fig. S75, ESI†), indicating that O_2 diffusion is inhibited by the methyl substituents on the phenyl moieties of the latter compounds compared to the former ones. The excited-state lifetime decay profile indicated that ultralong phosphorescence events last up to four and eight seconds for **5** and **7**, respectively (Fig. 4).

Crystal structures

A detailed analysis of the crystal structures of these compounds was carried out to get insight into the role of intermolecular interactions in the intriguing ultralong phosphorescence features. Compounds **1**, **3**, **4**, and **6** crystallize in the monoclinic crystal lattice with $P2_1/c$, $C2/c$, $C2/c$, and $P2_1/c$ space groups, respectively. Compounds **5** and **7** crystallize in the orthorhombic crystal system with the $Pbca$ space group, while **2** and **8** in the triclinic crystal system with the $P\bar{1}$ space group (Tables S2–S4, ESI†). The single crystal structures of **2**, **3**, **4**, and **6** were previously reported in the literature.[87–89] However, for the sake of consistency in the data analysis and meaningful interpretation of the optical features, we reproduced the crystal structures of **2**, **3**, **4**, and **6**.

Furthermore, the unit cell parameters and bond lengths (P–C and P═O) of **2**, **3**, **4**, and **6** are significantly different from those of previously reported structures (Tables S2–S4, ESI†).

Fig. 3 Fluorescence and phosphorescence spectra of the crystals of **5**: (a) λ_{ex} = 260 nm and (b) λ_{ex} = 340 nm; the crystals of **6**: (c) λ_{ex} = 260 nm and (d) λ_{ex} = 340 nm at 77 and 298 K under a N_2 atmosphere with a 100 µs delay. *A very weak phosphorescence signal was observed at 520 nm for **5** and **6** at 298 K (λ_{ex} = 340 nm).

This journal is © The Royal Society of Chemistry 2022

J. Mater. Chem. C, 2022, **10**, 9124–9131 | 9127

The phosphorus centers in **1–4** and **5–8** adopted trigonal pyramidal and tetrahedral geometry, respectively.[83,88–90] The P–C bond lengths in phosphines are found to be longer than the P–C bond ones in the corresponding phosphine oxides, which can be attributed to the greater lone pair–bond pair repulsive interactions in phosphines than the bond pair–bond pair interactions in phosphine oxides (Table S1, ESI†). Moreover, the dihedral angle between the aryl rings is considerably larger in phosphine oxides than that in phosphines (Table S1, ESI†). The P=O bond in **6** is significantly shorter than the values observed in other compounds.

In the crystal structure of **1**, intermolecular $(-C_6H_5)_3$P–H–C $(-C_6H_5)$ (2.979 Å) and $(-C_6H_5)$C-H-$\pi(-C_6H_5)$ (3.097 Å) interactions between adjacent molecules led to the formation of a 3D supramolecular structure. The intermolecular $(-CH_3)$C–H–π (3.513 Å), $(-C_6H_5)$C-H-$\pi(-C_6H_5)$ (2.828, 3.590 Å) and $(-C_6H_5)\pi-\pi(C_6H_5)$ interactions (average distance = $\sim$4.429, 4.468 Å) between adjacent molecules led to a 3D supramolecular structure in **2** (Fig. S35 and S36, ESI†). Multiple intermolecular interactions such as P=O–H–C$(-C_6H_5)$, $(-C_6H_5)$C-H-$\pi(-C_6H_5)$, $(-C_6H_5)$C-H-$\pi(-C_6H_5)$ and $(-CH_3)$C–H–π hold the molecules tightly in the crystal structures of phosphine oxides **5**, **6**, **7**, and **8** (Fig. S37–S39, ESI†).

It was found that the systematic changes in the steric perturbation around phosphorus atoms gradually reduced the number of P=O–H-C$(-C_6H_5)$ hydrogen bonding interactions per molecule in **5**, **6**, **7**, and **8**. For example, in **5**, P=O has trifurcated interactions with the CH of the $-C_6H_5$ moieties of three of its immediate neighbors in the solid state. In the crystal structure of **6**, the Ar_3P=O moiety showed bifurcated intermolecular interactions with the CH of the $-C_6H_5$ moiety of two of its immediate neighbors. In **7** and **8**, only one such type of interaction was observed. These results indicate that each methyl substituent on the aryl ring reduces one P=O–H-C $(-C_6H_5)$ interaction (Fig. S37–S39, ESI†). Further, the intermolecular C–H–π and π–π interactions between the aryl moieties of the adjacent molecules led to the formation of well-organized 3D supramolecular structures in the solids of **6**, **7**, and **8** (Fig. 5). These results indicate that the intermolecular interactions in crystalline phosphine oxides are more extensive than those in phosphines, which is one possible explanation for the ultralong phosphorescence characteristics of **5–8**.[90]

To understand the role of these intermolecular interactions in the ULRTP characteristics, PL and PXRD of ground samples of these compounds were studied in detail. The ground samples of these compounds showed both higher energy PL bands (fluorescence at 290, 291, 313, and 308 nm, respectively, for **5**, **6**, **7**, and **8**) and lower energy fluorescence bands, but no persistent luminescence band (480 nm to 550 nm) was observed at RT; however, the lower energy phosphorescence band recovered at 77 K (Fig. S76–S83, ESI†). The time-resolved decay kinetics of the ground samples of these compounds at RT does not show any decay corresponding to a lower energy phosphorescence band but recovered at 77 K (Table S8, ESI†). The PXRD patterns of the ground samples showed low intensity and broad diffraction peaks compared to the well-resolved
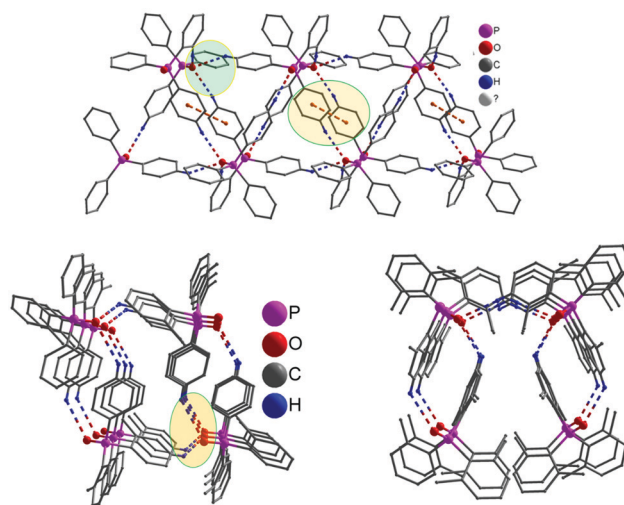

Fig. 5 Crystal structure of **5** showing intermolecular trifurcated P=O–H–C (blue circle) and π–π (orange circle) interactions (top). Crystal structure of **6** showing bifurcated P=O–H hydrogen bonding (bottom left). Crystal structure of **7** showing single P=O–H interactions (bottom right).

strong diffraction patterns obtained from pristine crystalline samples (Fig. S84, ESI†). This result indicates that the ground samples have smaller crystallites than the as-prepared crystalline solids. Based on these results, the lower energy luminescence bands in these compounds are attributed to the intermolecular aggregate emissions in the solid state.

To further validate the above conclusions, the PL spectra of thin films of these compounds were collected at RT and 77 K. The pristine solids and thin films of **1–4** did not show delayed emission features at room temperature. Interestingly, upon excitation at 260 nm, compounds **5–8** showed the PL band ($\sim$290–310 nm) corresponding to molecular species as observed for crystals and pristine samples (Fig. S85, ESI†). The PL spectra recorded at different excitation wavelengths suggest similar features (Fig. S86 and S87, ESI†). Further, the intramolecular phosphorescence bands recovered at low temperatures (Fig. S88 and S89, ESI†). Interestingly, the thin films of **5–8** did not show ultralong phosphorescence bands even at 77 K. Further, the excitation spectra of thin films of **5–8** did not show the band corresponding to intermolecular aggregates (Fig. S90, ESI†). These studies collectively implied that the intermolecular interactions are essential for ULRTP in compounds **5**, **6**, **7**, and **8**.

Theoretical studies

To gain more insight into the excited state electronic features, both singlet (S_1) and triplet (T_1) excited state geometries of these compounds were optimized and studied in detail (Fig. S92–S99 and Tables S10, S11, ESI†). Both S_1 and T_1 states are progressively stabilized when the steric crowding of the aryl moiety attached to the phosphorus center changes from phenyl → orthotolyl → xylyl ≈ mesityl moiety (Table S12, ESI†). In **5–8**, the P=O bond is elongated and the P–C bonds are shortened in the S_1 state compared to S_0 and T_1 states

9128 | *J. Mater. Chem. C*, 2022, **10**, 9124–9131

This journal is © The Royal Society of Chemistry 2022

(Fig. S100–S103 and Table S11, ESI†). The LSOMO of S_1 has contributions from the phosphorus atom in phosphine compounds and the oxygen atom in phosphine oxides. However, the HSOMO has no contributions from the heteroatoms (P and O) in both derivatives.

The orbital coefficient distributions in the LSOMO and HSOMO of the S_1 and T_1 states of 1–8 suggest weak intramolecular charge transfer in the excited states (Fig. S94–S99, ESI†). In T_1 of 5–8, one of the three aryl moieties attached to phosphorus deformed significantly from the planar structure (Fig. S100–S103 and Table S11, ESI†). This deformed ring is primarily involved in the LSOMO and HSOMO of these compounds. Unlike phosphine oxides, there is no deformation of the aryl moiety found in T_1 of phosphines 1–4 (Fig. S104–S107 and Table S10, ESI†). Moreover, S_1 in 1–4 is composed of mainly $n \rightarrow \pi^*$ transitions with weak CT characteristics. In contrast, T_1 in 1–4 is composed primarily of $\pi \rightarrow \pi^*$ transitions from the LSOMO to HSOMO.

S_1 and T_1 energy gaps were calculated using computed vertical transitions, and the values were estimated to be in the range of 0.64–1.43 eV. Although the $\Delta E_{S_1T_1}$ is significantly larger, higher triplet excited states T_5, T_4, T_4, T_4, T_{13}, T_{10}, T_{10}, and T_{13} are placed close to S_1 in 1–8, respectively (Fig. S108–S111, ESI†). Furthermore, dominant electronic configurations of S_1 matched well with these higher triplet excited states. Hence, these higher triplet excited states are involved in the ISC process from S_1, followed by internal conversion (IC) from $T_n \rightarrow T_1$. Phosphine oxides showed many possible intersystem crossing (ISC) channels than phosphine derivatives. This finding validates the efficient phosphorescence phenomenon observed for phosphine oxides 5–8 compared to 1–4.

The $\Delta E_{S_1T_1}$ values obtained from the experimental spectra (inter- and intramolecular species) and TD-DFT calculations are listed in Table S13 (ESI†). The $\Delta E_{S_1T_1}$ values obtained from intramolecular fluorescence and phosphorescence matched well with the computed $\Delta E_{S_1T_1}$ for monomers of 3, 4, 5, and 6. Further, the $\Delta E_{S_1T_1}$ calculated from excited state geometry optimizations of the monomers matched well with the experimental results obtained for 7 and 8. These results further strengthen our conclusion that the PL bands in the higher energy region correspond to the monomeric species, while the PL bands in the lower energy region are from the electronic states emerging from intermolecular aggregates.

Conclusion

In summary, we demonstrated the ULRTP properties of simple triarylphosphine oxides for the first time. The optical bandgap in these compounds can be fine-tuned by systematically varying the steric demanding of the aryl moiety attached to the phosphorus center. The repulsive interaction between the phosphorus lone pair electron and the attached π-system elevated the HOMO energies in 1–4 compared to phosphine oxides 5–8; consequently, phosphines absorb at a lower energy than the corresponding phosphine oxides. Phosphines 1–4 are better luminophores than phosphine oxides 5–8 in both solution and the solid state; however, phosphine oxides exhibit ULRTP with a lifetime exceeding 100 ms. Furthermore, ULRTP was observed only for the crystalline solids of 5–8 and was not observed for ground samples and thin films. A detailed solid-state structure and PXRD studies of 1–8 revealed that the strong C–H–O and C–H–π intermolecular interactions in crystalline phosphine oxides are more extensive than those in phosphines, which is one possible explanation for the ultralong phosphorescence characteristics of 5–8. A systematic steady-state and time-resolved photoluminescence (PL) and computational studies collectively affirmed that the intermolecular interactions are indeed crucial for ULRTP in these compounds. For the first time, these results show the promising potential of simple triarylphosphine/oxides for developing materials with RTP and ULRTP. The ULRTP quantum yields of these types of molecules can be improved by modifying the chemical constituents in these systems, which is being actively pursued in our laboratory.

Conflicts of interest

There are no conflicts to declare.

Acknowledgements

References

1 Y. Li, M. Gecevicius and J. Qiu, *Chem. Soc. Rev.*, 2016, **45**, 2090–2136.

2 E. Holder, B. M.-W. Langeveld and U. S. Schubert, *Adv. Mater.*, 2005, **17**, 1109–1121.

3 S. B. Zhao, T. McCormick and S. Wang, *Inorg. Chem.*, 2007, **46**, 10965–10967.

4 A. Pfister, G. Zhang, J. Zareno, A. F. Horwitz and C. L. Fraser, *ACS Nano*, 2008, **2**, 1252–1258.

5 G. Zhang, G. M. Palmer, M. W. Dewhirst and C. L. Fraser, *Nat. Mater.*, 2009, **8**, 747–751.

6 Q. Zhao, C. Huang and F. Li, *Chem. Soc. Rev.*, 2011, **40**, 2508–2524.

7 X. Chen, C. Xu, T. Wang, C. Zhou, J. Du, Z. Wang, H. Xu, T. Xie, G. Bi, J. Jiang, X. Zhang, J. N. Demas, C. O. Trindle, Y. Luo and G. Zhang, *Angew. Chem., Int. Ed.*, 2016, **55**, 9872–9987.

8 Kenry, C. Chen and B. Liu, *Nat. Commun.*, 2019, **10**, 1–5.

9 K. Jiang, Y. Wang, C. Cai and H. Lin, *Adv. Mater.*, 2018, **30**, 1800783.

10 H. Thomas, D. L. Pastoetter, M. Gmelch, T. Achenbach, A. Schlögl, M. Louis, X. Feng and S. Reineke, *Adv. Mater.*, 2020, **32**, 2000880.

11 S. Tian, H. Ma, X. Wang, A. Lv, H. Shi, Y. Geng, J. Li, F. Liang, Z. M. Su, Z. An and W. Huang, *Angew. Chem., Int. Ed.*, 2019, **131**, 6717–6721.

12 Z. Yang, Z. Mao, X. Zhang, D. Ou, Y. Mu, Y. Zhang, C. Zhao, S. Liu, Z. Chi, J. Xu, Y. C. Wu, P. Y. Lu, A. Lien and M. R. Bryce, *Angew. Chem., Int. Ed.*, 2016, **55**, 2181–2185.

13 S. M.-A. Fateminia, Z. Mao, S. Xu, Z. Yang, Z. Chi and B. Liu, *Angew. Chem., Int. Ed.*, 2017, **56**, 12160–12164.

14 Z. Wu, J. Nitsch, J. Schuster, A. Friedrich, K. Edkins, M. Loebnitz, F. Dinkelbach, V. Stepanenko, F. Wgrthner, C. M. Marian, L. Ji and T. B. Marder, *Angew. Chem., Int. Ed.*, 2020, **59**, 17137–17144.

15 M. Shimizu, R. Shigitani, M. Nakatani, K. Kuwabara, Y. Miyake, K. Tajima, H. Sakai and T. Hasobe, *J. Phys. Chem. C*, 2016, **120**, 11631–11639.

16 W. Jia, Q. Wang, H. Shi, Z. An and W. Huang, *Chem. – Eur. J.*, 2020, **26**, 4437–4448.

17 Y. Yu, M. S. Kwon, J. Jung, Y. Zeng, M. Kim, K. Chung, J. Gierschner, J. H. Youk, S. M. Borisov and J. Kim, *Angew. Chem., Int. Ed.*, 2017, **56**, 16207–16211.

18 W. J. Zhao, Z. K. He, J. W.-Y. Lam, Q. Peng, H. L. Ma, Z. G. Shuai, G. X. Bai, J. H. Hao and B. Z. Tang, *Chem*, 2016, **1**, 592–602.

19 Y. Lei, W. Dai, J. Guan, S. Guo, F. Ren, Y. Zhou, J. Shi, B. Tong, Z. Cai, J. Zheng and Y. Dong, *Angew. Chem., Int. Ed.*, 2020, **132**, 16188–16194.

20 B. T. Lim, S. Okajima, A. K. Chandra and E. C. Lim, *Chem. Phys. Lett.*, 1981, **79**, 22–27.

21 D. S. McClure, *J. Chem. Phys.*, 1949, **17**, 905–913.

22 A. Tsuboyama, H. Iwawak, M. Furugori, T. Mukaide, J. Kamatani, S. Igawa, T. Moriyama, S. Miura, T. Takiguchi, S. Okada, M. Hoshino and K. Ueno, *J. Am. Chem. Soc.*, 2003, **125**, 12971–12979.

23 Y. J. Su, H. L. Huang, C. L. Li, C. H. Chien, Y. T. Tao, P. T. Chou, S. Datta and R. S. Liu, *Adv. Mater.*, 2003, **15**, 884–888.

24 Y. You and S. Y. Park, *Dalton Trans.*, 2009, 1267–1282.

25 W. Lu, N. Zhu and C. M. Che, *J. Am. Chem. Soc.*, 2003, **125**, 16081–16088.

26 H. Rudmann, S. Shimada and M. F. Rubner, *J. Am. Chem. Soc.*, 2002, **124**, 4918–4921.

27 H. V.-R. Dias, H. V.-K. Diyabalanage, M. A.-R. Omary, M. A. Franzman and M. A. Omary, *J. Am. Chem. Soc.*, 2003, **125**, 12072–12073.

28 Q. Zhao, C. Huanga and F. Li, *Chem. Soc. Rev.*, 2011, **40**, 2508–2524.

29 H. Ma, Q. Peng, Z. An, W. Huang and Z. Shuai, *J. Am. Chem. Soc.*, 2019, **141**, 1010–1015.

30 Y. Xiong, Z. Zhao, W. Zhao, H. Ma, Q. Peng, Z. He, X. Zhang, Y. Chen, X. He, J. W.-Y. Lam and B. Z. Tang, *Angew. Chem., Int. Ed.*, 2018, **57**, 7997–8001.

31 Z. Chai, C. Wang, J. Wang, F. Liu, Y. Xie, Y. Z. Zhang, J. R. Li, Q. Li and Z. Li, *Chem. Sci.*, 2017, **8**, 8336–8344.

32 J. Yang, X. Zhen, B. Wang, X. Gao, Z. Ren, J. Wang, Y. Xie, J. Li, Q. Peng, K. Pu and Z. Li, *Nat. Commun.*, 2018, **9**, 840–849.

33 S. Mukherjee and P. Thilagar, *Chem. Commun.*, 2015, **51**, 10988–11003.

34 T. K. Sarkar, S. K. Sarkar and P. Thilagar, *ChemPhotoChem*, 2019, **4**, 282–286.

35 S. Jena, P. Dhanalakshmi, G. Bano and P. Thilagar, *J. Phys. Chem. B*, 2020, **124**, 5393–5406.

36 J. L. Ma, H. Liu, S. Y. Li, Z. Y. Li, H. Y. Zhang, Y. Wang and C. H. Zhao, *Organometallics*, 2020, **39**, 4153–4158.

37 L. Xu, G. Li, T. Xu, W. Zhang, S. Zhang, S. Yin, Z. Anc and G. He, *Chem. Commun.*, 2018, **54**, 9226–9229.

38 Z. Yang, Z. Mao, X. Zhang, D. Ou, Y. Mu, Y. Zhang, C. Zhao, S. Liu, Z. Chi, J. Xu, Y. C. Wu, P. Y. Lu, A. Lien and M. R. Bryce, *Angew. Chem., Int. Ed.*, 2016, **128**, 2221–2225.

39 Z. He, W. Zhao, J. W.-Y. Lam, Q. Peng, H. Ma, G. Liang, Z. Shuai and B. Z. Tang, *Nat. Commun.*, 2017, **8**, 416–423.

40 W. Z. Yuan, X. Y. Shen, H. Zhao, J. W.-Y. Lam, L. Tang, P. Lu, C. Wang, Y. Liu, Z. Wang, Q. Zheng, J. Z. Sun, Y. Ma and B. Z. Tang, *J. Phys. Chem. C*, 2010, **114**, 6090–6099.

41 S. Kothavale, W. J. Chung and J. Y. Lee, *ACS Appl. Mater. Interfaces*, 2020, **12**, 18730–18738.

42 J. Yang, M. Fang and Z. Li, *InfoMat*, 2020, **2**, 791–806.

43 L. Xu, G. Li, T. Xu, W. Zhang, S. Zhang, S. Yin, Z. Anc and G. He, *Chem. Commun.*, 2018, **54**, 9226–9229.

44 N. J. Turro, *Modern Molecular Photochemistry*, University Science Books, Mill Valley, 1991.

45 Z. An, C. Zheng, Y. Tao, R. Chen, H. Shi, T. Chen, Z. Wang, H. Li, R. Deng, X. Liu and W. Huang, *Nat. Mater.*, 2015, **14**, 685–690.

46 Z. Yang, Z. Mao, X. Zhang, D. Ou, Y. Mu, Y. Zhang, C. Zhao, S. Liu, Z. Chi, J. Xu, Y. C. Wu, P. Y. Lu, A. Lien and M. R. Bryce, *Angew. Chem., Int. Ed.*, 2016, **55**, 2181–2185 (*Angew. Chem.*, 2016, **128**, 2221–2225).

47 H. Mieno, R. Kabe, N. Notsuka, M. D. Allendorf and C. Adachi, *Adv. Optical Mater.*, 2016, **4**, 1015–1021.

48 Y. Shoji, Y. Ikabata, Q. Wang, D. Nemoto, A. Sakamoto, N. Tanaka, J. Seino, H. Nakai and T. Fukushima, *J. Am. Chem. Soc.*, 2017, **139**, 2728–2733.

49 Z. Wu, J. Nitsch, J. Schuster, A. Friedrich, K. Edkins, M. Loebnitz, F. Dinkelbach, V. Stepanenko, F. Wgrthner, C. M. Marian, L. Ji and T. B. Marder, *Angew. Chem., Int. Ed.*, 2020, **59**, 17137–17144.

50 M. Stolar and T. Baumgartner, *Chem. – Asian J.*, 2014, **9**, 1212–1225.

51 T. Baumgartner and R. Reau, *Chem. Rev.*, 2006, **106**, 4681–4727.

52 M. Stolar, J. B. Garcia, M. Toonen and T. Baumgartner, *J. Am. Chem. Soc.*, 2015, **137**, 3366–3371.

53 C. Fave, T. Y. Cho, M. Hissler, C. W. Chen, T. Y. Luh, C. C. Wu and R. Reau, *J. Am. Chem. Soc.*, 2003, **125**, 9254–9255.

54 F. Bu, E. Wang, Q. Peng, R. Hu, A. Qin, Z. Zhao and B. Z. Tang, *Chem. – Eur. J.*, 2015, **21**, 4440–4449.

55 E. Yamaguchi, C. Wang, A. Fukazawa, M. Taki, Y. Sato, T. Sasaki, M. Ueda, N. Sasaki, T. Higashiyama and S. Yamaguchi, *Angew. Chem., Int. Ed.*, 2015, **54**, 4539–4543.

56 T. Sanji, K. Shiraishi and M. Tanaka, *ACS Appl. Mater. Interfaces*, 2009, **1**, 1379–1382.

57 A. L. Von Ruden, L. Cosimbescu, E. Polikarpov, P. K. Koech, J. S. Swensen, L. Wang, J. T. Darsell and A. B. Padmaperuma, *Chem. Mater.*, 2010, **22**, 5678–5686.

58 P.-A. Bouit, A. Escande, R. Szucs, D. Szieberth, C. Lescop, L. Nyulaszi, M. Hissler and R. Reau, *J. Am. Chem. Soc.*, 2012, **134**, 6524–6527.

59 T. Hatakeyama, S. Hashimoto and M. Nakamura, *Org. Lett.*, 2011, **13**, 2130–2133.

60 Y. Matano, A. Saito, T. Fukushima, Y. Tokudome, F. Suzuki, D. Sa-kamaki, H. Kaji, A. Ito, K. Tanaka and H. Imahori, *Angew. Chem., Int. Ed.*, 2011, **123**, 8166–8170.

61 S. L. James, *Chem. Soc. Rev.*, 2009, **38**, 1744–1758.

62 M. Hidai, K. Tominari and Y. Uchida, *J. Am. Chem. Soc.*, 1972, **94**, 110–114.

63 R. Noyori, *Angew. Chem., Int. Ed.*, 2002, **41**, 2008–2022.

64 R. H. Grubbs, *Adv. Synth. Catal.*, 2007, **349**, 34–40.

65 M. Baudler and K. Glinka, *Chem. Rev.*, 1993, **93**, 1623–1667.

66 L. D. Quin, *A guide to organophosphorus chemistry*. John Wiley & Sons, 2000.

67 M. A. El-Sayed, *Acc. Chem. Res.*, 1968, **1**, 8–16.

68 Y. Tao, J. Xiao, C. Zheng, Z. Zhang, M. Yan, R. Chen, X. Zhou, H. Li, Z. An, Z. Wang, H. Xu and W. Huang, *Angew. Chem., Int. Ed.*, 2013, **52**, 10491–10495.

69 Y. Tao, L. Xu, Z. Zhang, R. Chen, H. Li, H. Xu, C. Zheng and W. Huang, *J. Am. Chem. Soc.*, 2016, **138**, 9655–9662.

70 H. Thomas, D. L. Pastoetter, M. Gmelch, T. Achenbach, A. Schlögl, M. Louis, X. Feng and S. Reineke, *Adv. Mater.*, 2020, **32**, 200088.

71 Y. Ning, J. Yang, H. Si, H. Wu, X. Zheng, A. Qin and B. Z. Tang, *Sci. China: Chem.*, 2021, **64**, 739–744.

72 G. R. Kumar and P. Thilagar, *Inorg. Chem.*, 2016, **55**, 12220–12229.

73 K. K. Neena, S. Pagidi and P. Thilagar, *Angew. Chem., Int. Ed.*, 2018, **57**, 16806–16810.

74 G. R. Kumar, S. K. Behera and P. Thilagar, *Dalton Trans.*, 2019, **48**, 6817–6823.

75 S. Pagidi, K. K. Neena and P. Thilagar, *Inorg. Chem.*, 2020, **59**, 3142–3151.

76 U. P. Pandey and P. Thilagar, *Adv. Optical Mater.*, 2020, **8**, 1902145.

77 U. P. Pandey, R. P. Nandi and P. Thilagar, *Front. Chem.*, 2020, **8**, 284–296.

78 R. P. Nandi, S. Pagidi, K. K. Neena and P. Thilagar, *Chem. – Eur. J.*, 2020, **26**, 16306–16317.

79 S. Jena, J. Eyyathiyil, S. K. Behera, M. Kitahara, Y. Imai and P. Thilagar, *Chem. Sci.*, 2022, **13**, 5893–5901.

80 S. Sasaki, F. Murakami and M. Yoshifuji, *Tetrahedron Lett.*, 1997, **38**, 7095–7098.

81 O. LarraÇaga, C. Romero-Nieto and A. de Cjzar, *Chem. – Eur. J.*, 2019, **25**, 9035–9044.

82 T. Baumgartner, *Acc. Chem. Res.*, 2014, **47**, 1613–1622.

83 P. Natarajan, *Anal. Methods*, 2014, **6**, 2432–2435.

84 Q. Peng, H. Ma and Z. Shuai, *Acc. Chem. Res.*, 2021, **54**, 940–949.

85 E. Lucenti, A. Forni, C. Botta, L. Carlucci, C. Giannini, D. Marinotto, A. Previtali, S. Righetto and E. Cariat, *J. Phys. Chem. Lett.*, 2017, **8**, 1894–1898.

86 W. Zhao, Z. He and B. Z. Tang, *Nat. Rev. Mater.*, 2020, **5**, 869–885.

87 T. S. Cameron and B. Dahlèn, *J. Chem. Soc., Perkin Trans. 2*, 1975, 1737–1751.

88 A. N. Sobolev, L. A. Chetkina, I. P. Room and E. N. Gur'yanova, *J. Struct. Chem.*, 1976, **17**, 83–88.

89 J. F. Blount, D. Camp, R. D. Hart, P. C. Healy, B. W. Skelton and A. H. White, *Aust. J. Chem.*, 1994, **47**, 1631–1639.

90 Q. Li and Z. Li, *Acc. Chem. Res.*, 2020, **53**, 962–973.

This journal is © The Royal Society of Chemistry 2022

J. Mater. Chem. C, 2022, **10**, 9124–9131 | **9131**